Radiolysis of cytosine at cryogenic temperatures by swift heavy ion bombardments

Gabriel Vignoli Muniz, Aditya Agnihotri, Basile Augé, Rafael Martinez, Christian Mejía, Hermann Rothard, Alicja Domaracka, Philippe Boduch

Radiolysis of Cytosine at Cryogenic Temperatures by Swift Heavy Ion Bombardments

Gabriel S. Vignoli Muniz[1,2,*], Aditya N. Agnihotri[1,3], Basile Augé[1,4], Rafael Martinez[5], Christian F.Mejía[6], Hermann Rothard[1], Alicja Domaracka[1], and Philippe Boduch[1]

[1]Centre de Recherche sur les Ions, les Matériaux et la Photonique. Normandie Université, ENSICAEN, UNICAEN, CEA, CNRS, CIMAP – 14000 Caen, France
[2]Instituto de Física, Universidade de São Paulo, Rua do Matão, 1371 – 05508-090, São Paulo, Brazil
[3]Indian Institute of Technology Delhi, New Dehli, India.
[4]Université Grenoble Alpes, CNRS, Institut de Planétologie et Astrophysique de Grenoble IPAG, Grenoble F-38041, France.
[5]Departamento de Física, Universidade Federal do Amapá, 22453-900 Macapá, Brazil.
[6]Facultad de Ciencias Quimicas, Universidad de Cuenca, Cuenca, Ecuador.

ABSTRACT: We investigated the radiolysis effects on the cytosine in the solid phase irradiated by swift heavy ions as galactic cosmic ray analogues (GCRs). Infrared (IR) absorption spectroscopy was employed to monitor the physical and chemical radiolytic modifications. The targets were prepared on ZnSe in two different ways: (1) by dropping a nucleobase−water−ethanol solution on the substrate and evaporating the solvent and (2) by sublimation of nucleobase powders in an oven and condensation on the windows. Both types of samples present similar IR absorption spectra. From the exponential decrease of the areas of IR absorption bands as a function of projectile fluence, apparent destruction cross sections (σ_d) were determined and were found to beery similar for samples prepared using both techniques. The destruction cross section of solid cytosine at cryogenic temperatures follows an electronic stopping (Se) power law: $\sigma d = C\ S_e^n$, where C is a constant and the exponential n is a dimensionless quantity. We determined $\sigma d = (3 \pm 1) \times 10^{-17}\ S_e^{(1.25 \pm 0.06)}$. New absorption features emerge from cytosine degradation, which can be attributed to OCN−, H2CO, and HNCO. By using the observed power law, the half-life of cytosine exposed to galactic cosmic rays was estimated in the order of Mega years. The findings reported here may help a better understanding of complex organic molecule radiostability.

1. INTRODUCTION

Nucleobases are aromatic heterocyclic compounds that contain nitrogen. Nucleobases are divided into two groups: purines, which include two heterocyclic fused rings, and pyrimidines, which contain a single heterocyclic ring such as cytosine (Figure 1). Nucleobases are crucial to the biosphere since they are building blocks of biomolecules such as deoxyribonucleic acid (DNA) and ribonucleic acid (RNA). These nucleic acids are responsible for the storage and transmission of genetic and hereditary information and responsible for the control of enzymatic cellular machinery. Nucleobases also play an important role in cell energy processing and cell signalization.[1] Moreover, they are components of daily human nutrition, for example, caffeine and vitamins B3 and B4; additionally, they are part of important medications.[2,3] Thus, a better understanding of nucleobase radiolysis can have relevance in medicine[4,5] and the areas of radiation processing of food and drugs.[6,7]

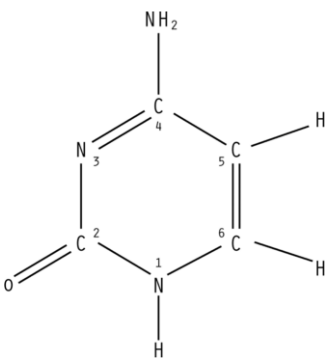

Figure 1. Schematic structure of cytosine molecules.

The presence of nucleobases in the meteorites found on Earth strongly indicates that this class of molecules can exist in outer space.[8−11] Albeit attempts to detect nucleobases in outer space by radio spectroscopy were fruitless.[12−14] Several chemical routes were proposed to form nucleobases from simple species present in outer space under astronomical conditions of cryogenic temperature and ionizing radia-tion.[15−19] Furthermore, experimental works mimicking astro-nomical environments revealed the formation of complex organic molecules including nucleobases.[16,20−25]

The omnipresent ionizing radiation field in space raises an important question if nucleobases are formed in astronomical

Table 1. Summary of Targets and Projectile Characteristics

sample	ion	energy (MeV)	electronic stopping power (MeV μm^{-1})	nuclear stopping power (10^{-3} MeV μm^{-1})	penetration depth (μm)	temperature (K)	thickness (μm)	column density (10^{17} cm^{-2})
cytosine grainy	Xe^{23+}	92	11.3	73	15.5	12	0.8	6.5
cytosine film	U^{32+}	116	13.4	250	16.7	12	0.34	2.8
cytosine film	Ni^{8+}	17	4.8	44	9.2	12	0.28	2.3
cytosine grainy	Ni^{8+}	17	4.8	44	9.2	12	0.20	1.6
cytosine grainy	Ca^{10+}	230	2.9	1.9	63	20	1.1	9.1

environments, can they survive the harsh conditions of outer space? Studying the radioresistance of nucleobases can give clues about their existence in outer space and even the possibility of their detection. Therefore, information about the radioresistance of nucleobases has pivotal importance in astrochemistry and astrobiology. Particularly, this could be relevant for the hypothesis of the RNA world; see more in.[26] In astrophysical environments, nucleobases are expected to exist in a low-temperature solid molecular matrix of water, CO_2, and NH_3.[27] As far as we know, a few experiments were performed under astrophysical conditions, *i.e.*, low temperature and solid phase. Adenine in a noble gas matrix was irradiated by 5 keV electrons.[28] Thymine with and without different water−ice contents was exposed to swift protons (0.8−1.0 MeV).[29] Uracil with different contents of water or CO_2 was irradiated by 0.9 MeV protons.[30] Nucleobases in a matrix of noble gas[31,32] and the pure solid phase (thin-film or solid samples)[33−38] were exposed to electromagnetic radiation.

In previous work, we investigated the radioresistance of solid adenine, a purine nucleobase, at low temperature exposed to swift heavy ions mimicking galactic cosmic rays (GCRs).[39]

In the present work, we investigated the radiolysis of solid cytosine at low temperatures (∼12 K) exposed to swift heavy ions. Cytosine was prepared in two different ways for which induced effects are found to differ at low doses, mostly correlated with structural rearrangement. From experiments using several heavy ion beams provided by Grand Accelerateur National d'Ions Lourds (GANIL) in Caen, France, and by Helmholtzzentrum für Schwerionenforschung (FAIR-GSI) in Darmstadt, Germany, we studied radiolysis as a function of the electronic stopping power of the ionic projectiles.

2. EXPERIMENTAL METHODOLOGY

2.1. Sample Preparation. Cytosine (≥98% pure) was purchased from Sigma-Aldrich. Cytosine powder was dissolved in a solution of ethanol and water (60.8% ethanol in water v/v) at a concentration of 1.5 mg mL^{-1}. The solution was exposed to ultrasound until all solid particles had visibly been dissolved. Then, drops of these solutions were applied directly onto windows of ZnSe (13 mm diameter, thickness 2 mm). The windows were heated up to 100 °C until the entire evaporation of the solvent, thus obtaining a solid sample. Hereafter, samples prepared in this manner will be referred to as "grainy" because of their grainy aspect under optical microscopy (see Figure S1 in the Supporting Information).

The second method was the preparation of uniform films from the sublimation of cytosine powder at low pressure (10^{-5} mbar) using an oven at 150 °C. A similar methodology was adopted by.[35−37] Optical microscopy and profilometry confirm that these samples are uniform thin films, henceforth for the sake of simplicity, we will refer to these samples as "films". The spectra of the nucleobase films are in good agreement with those reported in the literature, see Section 3.1, demonstrating that the process of heating does not destroy these molecules.

The preparation of nucleobase films from sublimation typically takes 3 or 4 h to produce a nucleobase film of a few hundred nanometers, whereas the production of grainy nucleobase samples is much faster, not taking longer than 20 min.

2.2. Sample Irradiation. Solid cytosine samples were irradiated at the beamline IRRSUD (17 MeV Ni^{8+}, 92 MeV Xe^{23+}, and 116 MeV U^{32+}) at GANIL (Caen, France) and the M-Branch of UNILAC (230 MeV Ca^{10+}) at FAIR-GSI (Darmstadt, Germany) in high vacuum chambers (10^{-8} mbar). The experiments at GANIL were performed in the CASIMIR setup described in detail elsewhere.[40] Each target was mounted on a cold finger connected to a closed cycle helium cold head equipped with a target heater, and the samples were irradiated at 12 K. The setup used in GSI is very similar, but it allows to mount of three samples inside the vacuum chamber; the irradiation temperature was slightly higher (≈20 K). For more details, see.[40,41] The average flux was about 10^9 ions cm^{-2} s^{-1} at IRRSUD and SME and 2×10^8 ions cm^{-2} s^{-1} at UNILAC.

The infrared (IR) absorption spectra were obtained *in situ* before and after irradiation with a Fourier transform infrared (FTIR) spectrometer (Nicolet Magna 550, Mercury Cadmium Telluride (MCT) detector cooled with liquid nitrogen), operating in transmission mode. The spectra were acquired as an average of 128 scans with wavenumbers ranging from 4000 to 700 cm^{-1} with a resolution of 2 cm^{-1}. The background of the bare window was taken at 12 K (20 K for GSI) and 300 K and used according to the temperature of the samples, thus avoiding thermal optics effects.

The projectile and target properties are summarized in Table 1. The electronic (S_e) and nuclear stopping (S_n) powers of the ionic projectiles in the solid nucleobase samples were calculated with the "Stopping and Ranges of Ions in Matter" (SRIM) software.[42] Note that for the swift projectiles used in this work, we are in the electronic regime of deposition of energy, $S_e \gg S_n$. Furthermore, the ion penetration depth is much larger than the sample thickness; therefore, there is no ion implantation in the solid nucleobase samples.

3. RESULTS AND DISCUSSION

3.1. Cytosine IR Absorption Spectra. Grainy and film cytosine samples display similar absorption spectra, Figure 2, in terms of band position but not in absorbance values (Table S1). Moreover, the absorption bands of the cytosine film are narrower than those of grainy cytosine samples. These minor

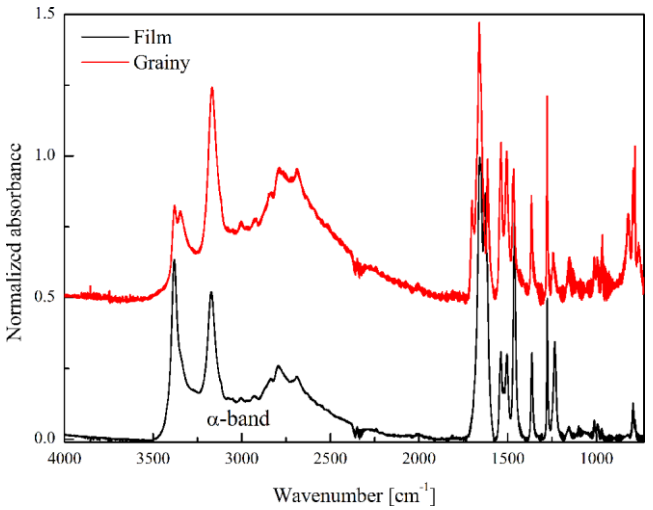

Figure 2. Normalized absorption spectra of grainy (red line) and film (black line) cytosine samples at room temperature. The grainy cytosine spectrum was shifted for clarity. The α-band (3500−2000 cm⁻¹) is indicated in the figure.

variations are plausibly due to the different microenvironments of the cytosine molecules.

Table 2 summarizes the absorption bands of grainy and film cytosine spectra, including the bands reported by[43] for cytosine in KBr pellets.

All of the nucleobases present a large IR absorption band between 3500 and 2000 cm^{-1} (the region containing characteristic vibration modes of C−H, N−H, and O−H). In the literature, this later region is called the α-band or β-band.[36,37] In this work, we will refer to this cytosine absorption band (3500−2000 cm^{-1}) as the "α-band". The grainy samples do not present a smooth surface (Figure S1). We estimated their thicknesses (d) considering the deposited mass (m) from the previously prepared cytosine solution. $d = m/\rho S$, where ρ is the cytosine density (1.5 g cm^{-3}) and S is the area of the ZnSe window (see Table 1).

3.2. Cytosine Film Thickness. Using a "Dektak 150 surfacer" profilometer from the Veeco brand in the GREYC laboratory (ENSICAEN, Caen, France), the thickness (d) and the roughness of cytosine film samples were measured. The samples were positioned in the center of the profilometer; using the microscope coupled to the profilometer, the profilometry tip was positioned onto a naked part of the ZnSe window. Then, the tip was moved throughout the sample, to determine the height between the ZnSe window and the edge of the film, thus giving us the thickness of the film. The thickness of each sample was determined as an average of four measurements (Table 1) corresponding to different scanned positions of the sample. A picture of a cytosine sample (film on the substrate window) and the corresponding measured profile are shown in Figure S2.

The cytosine column density (N) was determined as follows: $N = \frac{d\rho N_A}{MM} \times 10^{-4}$ [molecules cm^{-2}], where d is the film thickness, in μm, ρ is its density here assumed to be 1.5 g cm^{-3}, N_A is the Avogadro number, and MM is the cytosine molecular weight, 111.10 g mol^{-1}. To estimate the band strength (A-value) of a given IR absorption band, we used eq 1

$$A \text{ value} = \frac{\ln 10 A}{N} \quad (1)$$

Table 2. Comparison between Our Results and Those of[43]

assignment	vibration mode	position (cm^{-1})[43]	position (cm^{-1}) grainy cytosine	position (cm^{-1}) film cytosine
NH_2	antisymmetric stretching	3384	3381	3381
			3351	3349
NH_2	symmetric stretching	3180	3170	3173
		2840	2840	2863
CH	stretching	2796	2793	2794
CH	stretching	2690	2686	2688
NH_2	bending	1705	1703	
C_2O	stretching	1667	1660	1658
				1627
C_5=C_6	stretching	1616	1614	1615
NH	bending in plane	1540	1539	1538
$C_4$5N_3 and C_4−N_4	stretching	1505	1508	1506
C_4−N_3 and C_2−N_3	stretching	1469	1469	1463
C5C−H	bending	1366	1366	1365
C_2−N_1 and C_6−N_1	stretching	1280	1277	1276
C_4−N_4	stretching	1240	1242	1235
C−O	stretching	1155	1154	1157
NH_2	rocking mode	1100		1100
N_1−C_6−H	bending in plane	1012	1011	1010
C_4−C_5−H	bending in plane	995	996	993
C_4-C_5	stretching	966	967	961
NH	bending	822	820	825
ring	stretching breathing mode	794	793	794
		783	781	781
		758	762	
C_5−C_4−N_4	bending	700	700	703

Here, A is the integrated absorbance of a given IR feature and N is the column density. IR absorbance is measured on a log base-10 scale, therefore it is necessary to multiply the ratio between A and N by ln 10 to obtain the A-value. To evaluate the band strength, we used the determined thickness of three different samples. Thus, we estimate the A-value for the α-band as the (8.8 ± 0.7) × 10^{-16} cm $molecule^{-1}$. Additionally, we estimated the A-value for several cytosine absorption bands (Table S2). We would like to point out that the A-values estimated in this work are only valid for thin cytosine films with a thickness in the order of few hundred of nanometers.

3.3. Film Compaction. IR absorption spectroscopy is a suitable technique to follow the sample evolution during ion bombardment. It allows assessing the radiolytic destruction of cytosine, such as solid-phase transitions, radiolysis, sputtering, and formation of new chemical species.

Two cytosine samples were irradiated with the same projectile, 17 MeV Ni^{8+} (Table 1). Cytosine films (Figure 3a) present two different regimes with respect to target fluences. Note that the integrated absorbance at 1539 cm^{-1} increases at low fluences, $F < 6.0 \times 10^{10}$ cm^{-2}; however, at higher fluences, the integrated absorbance decreases exponentially.

The increase of integrated absorbance is correlated with the compaction process of cytosine films, *i.e.*, structural rearrangement of cytosine molecules by the irradiation, and the

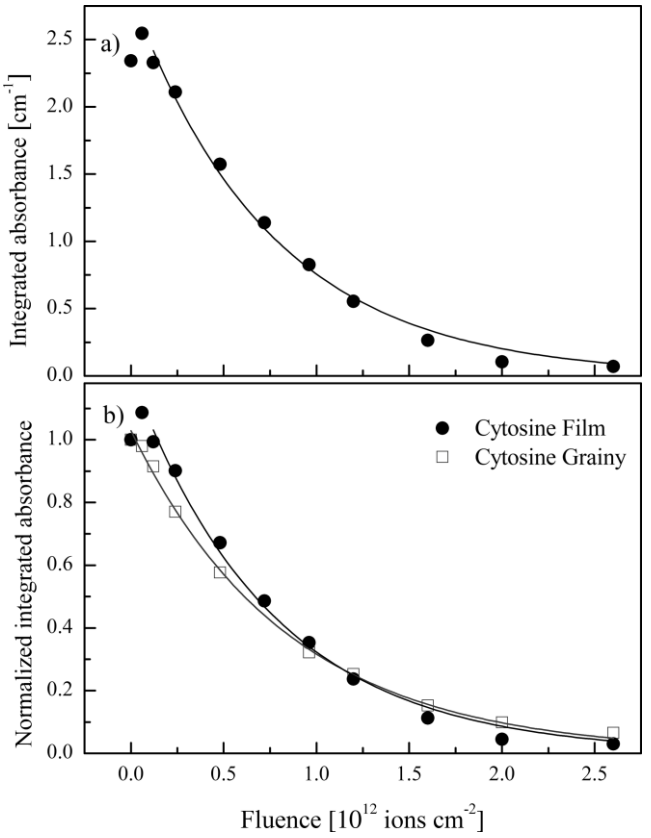

Figure 3. Integrated absorbance at 1539 cm^{-1} of cytosine films as a function of the fluence of 17 MeV Ni^{8+} (a). Normalized integrated absorbance at 1539 cm^{-1} of the film (black circles) and grainy (open squares) cytosine samples as a function of the fluence of 17 MeV Ni^{8+} (b).

subsequent changes in the band strength.[40,44] Assuming that the cytosine column density does not change much at low fluences, it is feasible to estimate the variation in the band strength induced by the film compaction. Under this assumption, the variation of the band strength at 1539 cm^{-1} is 8%. Interestingly, the compaction effects are unobserved for grainy samples, and that cytosine decay is very similar in both film and grainy samples (Figure 3b).

3.4. Cytosine Radiolysis. Henceforth, we studied cytosine radiolysis at cryogenic temperatures with the electronic energy loss ranging from 2.9 to 13.4 MeV μm^{-1}. For this task, we used two facilities with two similar setups and three different ion beamlines (GANIL and GSI).

We observe that for doses higher than 0.35 eV per molecule, the overall IR absorption intensity decreases exponentially with the accumulated number of projectiles (fluence). For example, Figure 4 displays the evolution of grainy and film cytosine samples bombarded by 17 MeV Ni^{8+} at 12 K.

The decrease of the IR absorbance values is due to the disappearance of the initial molecule caused by either destruction or sputtering. Both effects, destruction and sputtering, can be quantified by introducing the apparent destruction cross section (σ_d); σ_d is defined as a sum between the molecule destruction cross section and the sputtering per incoming ion. For more details, see.[39,45,46]

The integrated absorbance (A) evolution as an ion fluence function can be written according to eq 2

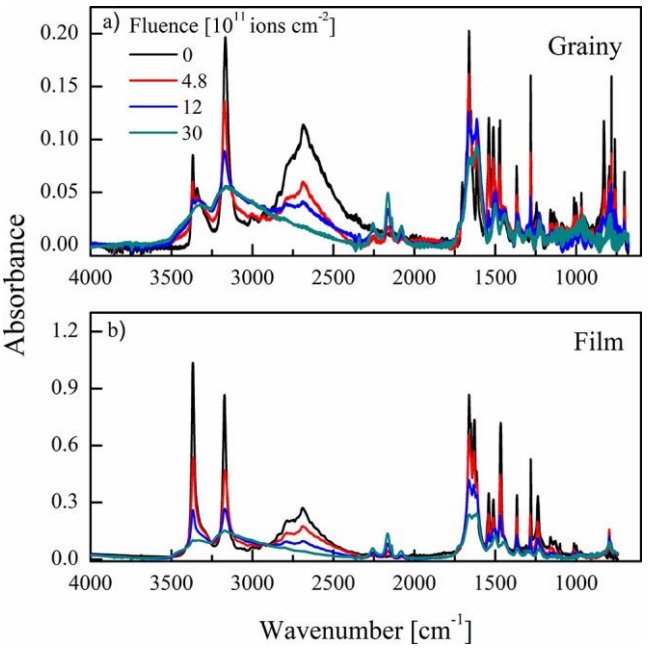

Figure 4. Spectra of grainy (a) and film (b) cytosine samples at 12 K. The samples were irradiated by 17 MeV Ni^{8+} at different fluences.

$$A = A_0 e^{-\sigma_d F} \quad (2)$$

where F is the fluence and A_0 is the initial integrated absorbance of a given IR band.

Figure 5 displays the evolution of the normalized integrated absorbance at 1539 cm^{-1} as a function of the accumulated ions

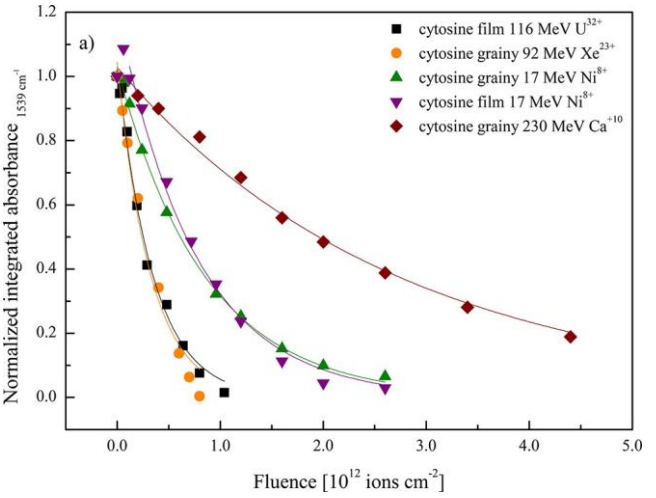

Figure 5. Normalized integrated absorbance at 1539 cm^{-1} as a function of the projectile fluence. The full lines correspond to the fitting of the data with eq 2.

per square centimeter. This figure shows that the projectiles with higher electronic energy loss (Table 1) cause a faster and stronger decay of the IR integrated absorbance.

The evolution of several absorption bands was monitored during the heavy ion bombardment, and the respective destruction cross sections were determined by fitting eq 2(see Table 3). The IR feature at 1539 cm^{-1} yielded the highest cross section values (Table S3). It is important to mention that, in principle, all of the bands should yield the

Table 3. Destruction Cross Sections of Cytosine for Different Projectiles

projectile	σ_d [10^{-12} cm^2]	sample
116 MeV U^{32+}	(3.50 ± 0.09)	film
92 MeV Xe^{23+}	(3.0 ± 0.3)	grainy
17 MeV Ni^{8+}	(1.17 ± 0.03)	grainy
17 MeV Ni^{8+}	(1.31 ± 0.06)	film
230 MeV Ca^{10+}	(0.51 ± 0.01)	grainy

same cross section values. We speculate that the different cross section values are due to the presence of IR absorption features from the radioproducts and/or the changes in the band strength induced by the irradiation and the subsequent changes in cytosine's local chemical environment. Therefore, for our calculations, we will use the highest cross section values, that is, the cross sections determined from the decay of the IR absorption band at 1539 cm^{-1} (Table 3).

Note that grainy and film cytosine samples were irradiated by the same projectiles (17 MeV Ni^{8+}) leading to very similar cross sections (Tables 3 and S3).

As pointed out by,[47] it has been reported, for more than four decades, that the destruction cross sections for swift ions follow a power law on the electronic stopping power under the form $\sigma_d = C\, S_e^n$, where C is a constant and n is a dimensionless quantity. Additionally, it has been observed that the parameter n ranges from 1.0 to 1.5 for different molecules; for more details, see[47,48] and the references therein.

Figure 6 shows the destruction cross section of cytosine as a function of the electronic stopping power by using the following power law: $\sigma_d = C\, S_e^n$.

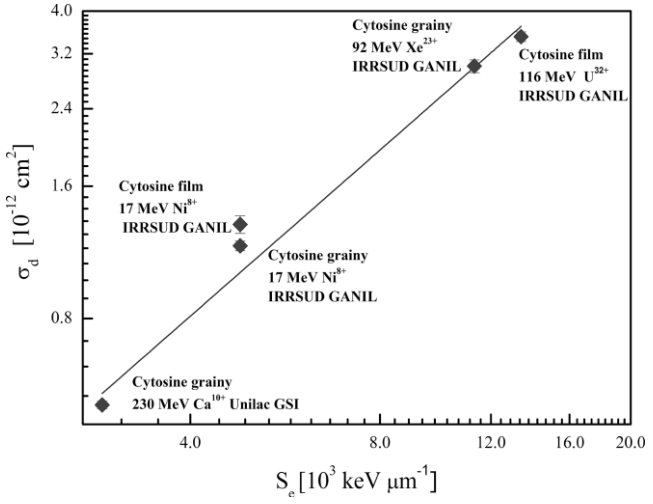

Figure 6. Apparent destruction cross section of cytosine as a function of the electronic stopping power.

The best fitting processes yielded $\sigma_d = (3 \pm 1) \times 10^{-17} S_e^{(1.25\pm0.06)}$ with S_e in keV μm^{-1} for σ_d in cm^2. The fitting yielded a $\chi^2 = 0.97$.

3.5. Radioproducts: New Molecules from Cytosine Radiolysis. Although the goal of this paper is not to investigate the radioproducts from cytosine degradation, we observed that swift ion irradiation not only leads to the decrease in nucleobase IR absorption lines, but new absorption bands arise in the IR spectra. We will highlight the new absorption bands and possible candidates for these IR bands. Cytosine displays a very complex vibrational spectrum, making it hard to identify the molecules responsible for the new absorption features unequivocally. It is nevertheless possible to propose that some candidates of new molecular species are responsible for the observed absorption. We observe that new absorption features emerge from all nucleobase spectra due to sample radio degradation.

Grainy and film samples exhibit the same new absorption features for the same deposited local dose. Figure 7 displays the evolution of the IR absorption spectra of cytosine before and during the bombardment by 116 MeV U^{32+} at different fluences. The IR spectra were shifted for better visualization.

The energetic processing of cytosine samples produced new absorption bands in the region of 2300−2000 cm^{-1} (Figure 7a). Note that cytosine does not display absorption peaks in that region; this region is characteristic of nitrile and isonitrile vibrations.[49]

At lower wavenumbers (Figure 7b), small peaks emerge between 1720 and 1500 cm^{-1}, which can be attributed to H_2CO,[45,50] as indicated in Figure 7b.

To identify the radioproducts, the absorption band between 2300 and 2000 cm^{-1} was deconvoluted (Figure 8c). The following absorption peaks are observed: 2077, 2138, 2164, 2227, and 2256 cm^{-1}. The FWHH of the absorption peak at 2139 cm^{-1} is 4.4 cm^{-1}; accordingly, this seems to be the IR absorption peak of CO.[51] The absorption band at 2165 cm^{-1} may be assigned to OCN^-.[52] Indeed, the formation of OCN^- from the destruction of the cytosine ring is plausible (see Figure 1). The absorption band at 2258 cm^{-1} is attributed to HNCO.[32,53]

4. ASTROPHYSICAL IMPLICATIONS

From the astrophysical point of view, it is important to estimate the half-life ($\tau_{1/2}$) of molecules exposed to ionizing radiation fields. This can indicate the probability of detecting a given molecule in an astronomical environment and the possibility of a molecule composing the inventory of molecules in a planetary disk.

To estimate the half-life of solid cytosine exposed to galactic cosmic rays (GCRs), we calculate the cytosine destruction rate, *i.e.*, the product of the destruction cross section, and the flux of cosmic rays. We selected the 10 most-abundant ions that compose the GCRs and determined the destruction cross section as a function of the energy per nucleon (E) using the code SRIM[55] and the observed power law (see Section 3.4 (Figure S3)). As expected, heavier elements display higher destruction cross sections since, for swift ions, the stopping power is proportional to the square of the projectile atomic number and approximately inversely proportional to the square of the projectile velocity.[54,55]

The distribution of cosmic rays ($\Phi(Z, E)$) is well-determined at energies above 1 GeV per nucleon (GeV/n). Though, the differential flux at low energies is less accurate, due to the interaction between the charged particles, the heliosphere, and the planetary magnetic fields.[56] In this work, the GCR differential flux was calculated using the model proposed by[56,57] according to eq 3.

$$\Phi(Z, E) = C(Z)E^{0.3}/(E_0 + E)^3 \quad (3)$$

$C(Z)$ is a normalization constant. The numerical values of $C(Z)$ were adapted from[58] (see Table S4). In this model, E_0 is a parameter that modulates the differential fluxes only at low

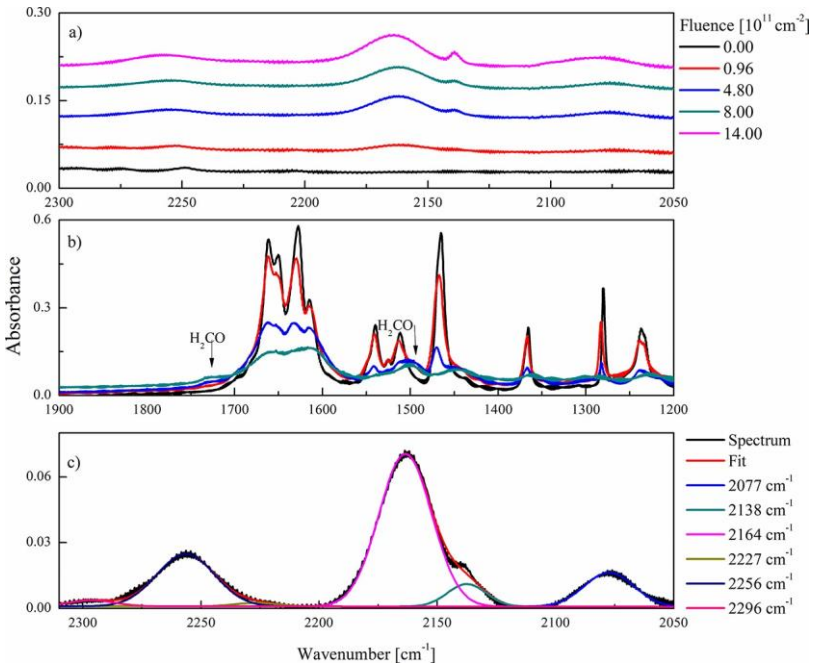

Figure 7. IR spectra of the cytosine film irradiated by 116 MeV U^{32+} at different fluences. The sample was irradiated by 116 MeV U^{32+} at different fluences, within wavenumbers ranging from 2300 to 2050 cm^{-1} (a) and from 1900 to 1200 cm^{-1} (b). Deconvolution of the band between 2300−2050 cm^{-1} of the cytosine film irradiated by 116 MeV U^{32+} at the fluence of 1.44×10^{12} ions cm^{-2} (19.6 eV per molecule) at 12 K (c).

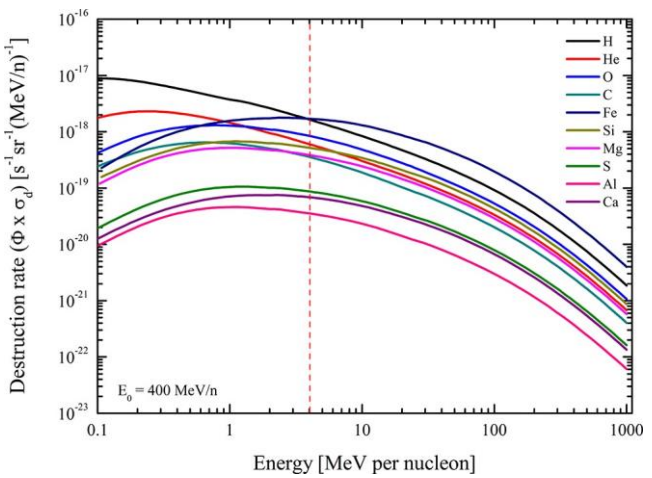

Figure 8. Cytosine destruction rate for the 10 most-abundant elements of the galactic cosmic rays as an energy function. The dashed red line is only a guide for the eyes. E_0 = 400 MeV/n.

energies but does not have an impact at high energies. E_0 values range from 0 to 940 MeV/n. It was shown that the E_0 = (300 ± 100) MeV/n is the best parameter to explain the $^3He/^4He$ measured ratio.[57] Here, we decided to investigate how different E_0 values, namely, 200, 400, and 600 MeV/n, would impact the cytosine half-live. Therefore, here we adopted these three values for the E_0 parameter to simulate the GCR fluxes and estimate the half-live of cytosine exposed to GCRs. Figure S4 shows the GCRs calculated using these three values of the parameter E_0.

The cytosine destruction rate ($\sigma_d(Z, E) \times \Phi(Z, E)$) is exhibited in Figure 8. Interestingly, at energies higher than 4 MeV/n, iron is the most effective element to destroy cytosine (see the red dashed line in Figure 8). Note that in the energy range of 4−1000 MeV/n, iron displays cross sections about 4 orders of magnitude higher than hydrogen (Figure S3), thus iron compensates for its low abundance and becomes the most efficient cosmic ray element to destroy cytosine.

The half-life of cytosine can be calculated by $\tau_{1/2}(Z) = \ln 2/(4\pi \Sigma_Z \int \sigma_d(E,Z)\Phi(E,Z)\,dE)$, and the integral was performed from 0.1 to 1000 MeV/n. The factor 4π is due to the fact that the GCR flux is isotropic; however, this value is small in comparison with the uncertainties of the GCR distribution (see Figure S4). For the total half-life, it is necessary to perform a summation of each element. Table 4 displays the half-life of cytosine exposed to cosmic rays for distinct values of E_0. It is important to point out that the values here are only an estimation given the uncertainties of the GCR flux.

Table 4. Half-life of Cytosine Exposed to Cosmic Rays for Different Values of the Parameter E_0

E_0 (MeV/n)	$\tau_{1/2}$ (Myears)
200	1.2
400	7.3
600	20.5

Taking into consideration the same GCR distributions, cytosine was found slightly more radio susceptible than adenine.[39] Indeed, more experimental and theoretical approaches are necessary to better understand the susceptibility of purine and pyrimidine nucleobases to ionizing radiation.

5. CONCLUSIONS

In this work, the processing of solid cytosine at cryogenic temperatures by swift heavy ions was investigated. Cytosine targets were produced by two different methods: (1) by dropping a water−ethanol nucleobase solution on ZnSe windows followed by heating and solvent evaporation and

(2) by sublimation of the nucleobase and condensation on a ZnSe window. This latter method produces a thin smooth solid nucleobase film. By using profilometry and combining with IR data, band strengths for several IR absorption bands of the cytosine film were estimated at room temperature, with the α-band (3500− 2000 cm^{-1}) presenting an A-value that equals $(8.8 \pm 0.7) \times 10^{-16}$ cm $molecule^{-1}$.

At low fluences ($F < 1 \times 10^{11}$ cm^{-2}), cytosine films present an increase in the IR absorbance; this is probably correlated with molecular rearrangement and changes in their band strength. For both types of samples, film and grainy, the evolution of the IR spectra under heavy ion bombardment is very similar, yielding destruction cross sections equal within error bars. Furthermore, as observed for many organic molecules, cytosine destruction cross section follows an electronic stopping (S_e) power law under the form: $(3 \pm 1) \times 10^{-17}$ $S_e^{(1.25\pm0.06)}$. The half-life of cytosine exposed to GCRs was estimated using different GCR fluxes; the values estimated here are in order of Mega years. The results here suggest that the search for nucleobases by radio spectroscopy should be performed.

ACKNOWLEDGMENTS

This work was supported by Brazilian agencies CNPq (INEspaço and Science without Borders) and FAPERJ, as well as the CAPES-COFECUB French-Brazilian exchange program, the European Commission, FP7 for RTD Capacities Programme (Contract No. 262010, ENSAR), and the EU's Horizon 2020 Research and Innovation Programme (grant agreement no. 654002 ENSAR2). It is a pleasure to thank Thierry Been, Jean-Marc Ramillon, Toiammou Madi, and Dr. Clara Grygiel for their invaluable support. The authors wish to acknowledge the staff of GANIL and GSI for their invaluable help throughout the course of the experiments. The authors are particularly thankful to Prof. Dr. Christina Trautmann, Dr. Daniel Severin, Dr. Markus Bender, Alexander Warth, and Arne Siegmund at GSI. The experiments were performed at *Grand Accélérateur National d'Ions Lourds* (GANIL) Caen, France, and at (GSI) *Helmholtzzentrum für Schwerionenforschung*, Darmstadt, Germany. The authors also thank the reviewers for their constructive remarks.

REFERENCES

(1) Molecular Biology of the Cell, 5th ed.; Alberts, B., Ed.; Garland Science: New York, 2008.

(2) Girke, C.; Daumann, M.; Niopek-Witz, S.; Möhlmann, T. Nucleobase and Nucleoside Transport and Integration into Plant Metabolism. Front. Plant Sci. 2014, 5, No. 443.

(3) Yssel, A. E. J.; Vanderleyden, J.; Steenackers, H. P. Repurposing of Nucleoside- and Nucleobase-Derivative Drugs as Antibiotics and Biofilm Inhibitors. J. Antimicrob. Chemother. 2017, 72, 2156−2170.

(4) Jäkel, O.; Schulz-Ertner, D.; Karger, C. P.; Nikoghosyan, A.; Debus, J. Heavy Ion Therapy: Status and Perspectives. Technol. Cancer Res. Treat. 2003, 2, 377−387.

(5) Pompos, A.; Durante, M.; Choy, H. Heavy Ions in Cancer Therapy. JAMA Oncol. 2016, 2, 1539.

(6) Silindir, M.; Ozer, Y. The Effect of Radiation on a Variety of Pharmaceuticals and Materials Containing Polymers. PDA J. Pharm. Sci. Technol. 2012, 66, 184−199.

(7) Diehl, J. F. Food Irradiation Past, Present and Future. Radiat. Phys. Chem. 2002, 63, 211−215.

(8) Shimoyama, A.; Hagishita, S.; Harada, K. Search for Nucleic Acid Bases in Carbonaceous Chondrites from Antarctica. *Geochem. J.* 1990, *24*, 343 − 348.

(9) Martins, Z.; Botta, O.; Fogel, M. L.; Sephton, M. A.; Glavin, D. P.; Watson, J. S.; Dworkin, J. P.; Schwartz, A. W.; Ehrenfreund, P. Extraterrestrial Nucleobases in the Murchison Meteorite. *Earth Planet. Sci. Lett.* 2008, *270*, 130 − 136.

(10) Callahan, M. P.; Smith, K. E.; Cleaves, H. J.; Ruzicka, J.; Stern, J. C.; Glavin, D. P.; House, C. H.; Dworkin, J. P. Carbonaceous Meteorites Contain a Wide Range of Extraterrestrial Nucleobases. *Proc. Natl. Acad. Sci. U.S.A.* 2011, *108*, 13995 − 13998.

(11) Smith, K. E.; Callahan, M. P.; Gerakines, P. A.; Dworkin, J. P.; House, C. H. Investigation of Pyridine Carboxylic Acids in CM2 Carbonaceous Chondrites: Potential Precursor Molecules for Ancient Coenzymes. *Geochim. Cosmochim. Acta* 2014, *136*, 1 − 12.

(12) Kuan, Y.-J.; Yan, C.-H.; Charnley, S. B.; Kisiel, Z.; Ehrenfreund, P.; Huang, H.-C. A Search for Interstellar Pyrimidine. *Mon. Not. R. Astron. Soc.* 2003, *345*, 650 − 656.

(13) Kuan, Y.-J.; Charnley, S. B.; Huang, H.-C.; Kisiel, Z.; Ehrenfreund, P.; Tseng, W.-L.; Yan, C.-H. Searches for Interstellar Molecules of Potential Prebiotic Importance. *Adv. Space Res.* 2004,
33, 31 − 39.

(14) Brünken, S.; McCarthy, M. C.; Thaddeus, P.; Godfrey, P. D.; Brown, R. D. Improved Line Frequencies for the Nucleic Acid Base Uracil for a Radioastronomical Search. *Astron. Astrophys.* 2006, *459*, 317 − 320.

(15) Roy, D.; Najafian, K.; von Rague Schleyer, P. Chemical Evolution: The Mechanism of the Formation of Adenine under Prebiotic Conditions. *Proc. Natl. Acad. Sci. U.S.A* 2007, *104*, 17272 − 17277.

(16) Saladino, R.; Crestini, C.; Pino, S.; Costanzo, G.; Di Mauro, E. Formamide and the Origin of Life. *Phys. Life Rev.* 2012, *9*, 84 − 104.

(17) Ricca, A. A Computational Study of the Mechanisms for the Incorporation of a Nitrogen Atom into Polycyclic Aromatic Hydrocarbons in the Titan Haze. *Icarus* 2001, *154*, 516 − 521.

(18) da Silva, J. B. P.; de Araujo, A. P. M. A New Mechanism of Guanine-Isomer Formation from Species Previously Observed in the Interstellar Medium. *ACS Earth Space Chem.* 2017, *1*, 376 − 383.

(19) Chakrabarti, S. K.; Majumdar, L.; Das, A.; Chakrabarti, S. Search for Interstellar Adenine. *Astrophys. Space Sci.* 2015, *357*, No. 90.

(20) Horst, S.; Yelle, R. V.; Buch, A.; Carrasco, N.; Cernogora, G.;
Dutuit, O.; Quirico, E.; Sciamma-O′Brien, E.; Smith, M. A.; Somogyi, A..; Szopa, C.; Thissen, R.; Vuitton, V. Formation of Amino Acids and Nucleotide Bases in a Titan Atmosphere Simulation Experiment. *Astrobiology* 2012, *12*, 809 − 817.

(21) Nuevo, M.; Chen, Y.-J.; Hu, W.-J.; Qiu, J.-M.; Wu, S.-R.; Fung, H.-S.; Chu, C.-C.; Yih, T.-S.; Ip, W.-H.; Wu, C.-Y. R. Irradiation of Pyrimidine in Pure H 2 O Ice with High-Energy Ultraviolet Photons. *Astrobiology* 2014, *14*, 119 − 131.

(22) Ada Bibang, P. C. J.; Agnihotri, A. N.; Auge, B.; Boduch, P.; Desfrançois, C.; Domaracka, A.; Lecomte, F.; Manil, B.; Martinez, R.; Muniz, G. S. V.; Nieuwjaer, N.; Rothard, H. Ion Radiation in Icy Space Environments: Synthesis and Radioresistance of Complex Organic Molecules. *Low Temp. Phys.* 2019, *45*, 590 − 597.

(23) Cottin, H.; Kotler, J. M.; Bartik, K.; Cleaves, H. J.; Cockell, C. S.; de Vera, J.-P. P.; Ehrenfreund, P.; Leuko, S.; Ten Kate, I. L.;
Martins, Z.; Pascal, R.; Quinn, R.; Rettberg, P.; Westall, F. Astrobiology and the Possibility of Life on Earth and Elsewhere. *Space Sci. Rev.* 2017, *209*, 1 − 42.

(24) Materese, C. K.; Nuevo, M.; Sandford, S. A. The Formation of Nucleobases from the Ultraviolet Photoirradiation of Purine in Simple Astrophysical Ice Analogues. *Astrobiology* 2017, *17*, 761 − 770.

(25) Pilling, S.; Andrade, D. P. P.; Neto, A´C.; Rittner, R.; Naves de Brito, A. DNA Nucleobase Synthesis at Titan Atmosphere Analog by Soft X-Rays. *J. Phys. Chem. A* 2009, *113*, 11161 − 11166.

(26) Higgs, P. G.; Lehman, N. The RNA World: Molecular Cooperation at the Origins of Life. *Nat. Rev. Genet.* 2015, *16*, 7 − 17.

(27) Oba, Y.; Takano, Y.; Naraoka, H.; Watanabe, N.; Kouchi, A. Nucleobase Synthesis in Interstellar Ices. *Nat. Commun.* 2019, *10*, No. 4413.

(28) Evans, N. L.; Bennett, C. J.; Ullrich, S.; Kaiser, R. I. On the interaction of adenine with ionizing radiation: mechanistical studies and astrobiological implications. *Astrophys. J.* 2011, *730*, 69.

(29) Materese, C. K.; Gerakines, P. A.; Hudson, R. L. The Radiation Stability of Thymine in Solid H2O. *Astrobiology* 2020, *20*, 956 − 963.

(30) Gerakines, P. A.; Qasim, D.; Frail, S.; Hudson, R. L. Radiolytic Destruction of Uracil in Interstellar and Solar System Ices.
Astrobiology 2022, *22*, 233 − 241.

(31) Peeters, Z.; Botta, O.; Charnley, S. B.; Kisiel, Z.; Kuan, Y.-J.; Ehrenfreund, P. Formation and Photostability of N-Heterocycles in Space: I. The Effect of Nitrogen on the Photostability of Small Aromatic Molecules. *Astron. Astrophys.* 2005, *433*, 583 − 590.
(32) Peeters, Z.; Botta, O.; Charnley, S. B.; Ruiterkamp, R.; Ehrenfreund, P. The Astrobiology of Nucleobases. *Astrophys. J.* 2003, *593*, L129 − L132.
(33) Poch, O.; Kaci, S.; Stalport, F.; Szopa, C.; Coll, P. Laboratory Insights into the Chemical and Kinetic Evolution of Several Organic Molecules under Simulated Mars Surface UV Radiation Conditions. *Icarus* 2014, *242*, 50 − 63.
(34) Pilling, S.; Andrade, D. P. P.; do Nascimento, E. M.; Marinho, R. R. T.; Boechat-Roberty, H. M.; de Coutinho, L. H.; de Souza, G. G. B.; de Castilho, R. B.; Cavasso-Filho, R. L.; Lago, A. F.; de Brito, A. N. Photostability of Gas- and Solid-Phase Biomolecules within Dense Molecular Clouds Due to Soft X-Rays: Photostability of Biomolecules in ISM. *Mon. Not. R. Astron. Soc.* 2011, *411*, 2214 − 2222.
(35) Guan, Y. Y.; Fray, N.; Coll, P.; Macari, F.; Chaput, D.; Raulin, F.; Cottin, H. UVolution: Compared Photochemistry of Prebiotic Organic Compounds in Low Earth Orbit and in the Laboratory. *Planet. Space Sci.* 2010, *58*, 1327 − 1346.
(36) Saiagh, K.; Cottin, H.; Aleian, A.; Fray, N. VUV and Mid-UV Photoabsorption Cross Sections of Thin Films of Guanine and Uracil: Application on Their Photochemistry in the Solar System. *Astrobiology* 2015, *15*, 268 − 282.
(37) Saiagh, K.; Cloix, M.; Fray, N.; Cottin, H. VUV and Mid-UV Photoabsorption Cross Sections of Thin Films of Adenine: Application on Its Photochemistry in the Solar System. *Planet. Space Sci.* 2014, *90*, 90 − 99.
(38) Rouquette, L.; Stalport, F.; Cottin, H.; Colas, C.; Georgelin, T.; Chaouche-Mechidal, N.; Lasne, J.; Mahfouf, S.; Raulin, F.; Selliez, L.; Szopa, C.; Coll, P. Dimerization of Uracil in a Simulated Mars-like UV Radiation Environment. *Astrobiology* 2020, *20*, 1363 − 1376.
(39) Vignoli Muniz, G. S.; Mejia, C. F.; Martinez, R.; Auge, B.; Rothard, H.; Domaracka, A.; Boduch, P. Radioresistance of Adenine to Cosmic Rays. *Astrobiology* 2017, *17*, 298 − 308.
(40) Mejia, C.; de Barros, A. L. F.; Seperuelo Duarte, E.; da Silveira, E. F.; Dartois, E.; Domaracka, A.; Rothard, H.; Boduch, P. Compaction of Porous Ices Rich in Water by Swift Heavy Ions. *Icarus* 2015, *250*, 222 − 229.
(41) Severin, Daniel.; Trautmann, Christina.; Neumann, Reinhard. The MBranch, a New UNILAC Irradiation Facility with in-Situ Analytical Techniques for Materials Research *GSI Sci. Rep.* 2008.
(42) Ziegler, J. F.; Ziegler, M. D.; Biersack, J. P. *SRIM*, www.srim.com2012.
(43) Mathlouthi, M.; Seuvre, A. M.; Koenig, J. L. F.T.-I.R. and Laser- Raman Spectra of Cytosine and Cytidine. *Carbohydr. Res.* 1986, *146*, 1 − 13.
(44) Costa, C. A. P. d.; da Muniz, G. S. V.; Boduch, P.; Rothard, H.; Silveira, E. F. da. Valine Radiolysis by H^+, He^+, N^+, and S^{15+} MeV Ions. *Int. J. Mol. Sci.* 2020, *21*, 1893.
(45) de Barros, A. L. F.; Boduch, P.; Domaracka, A.; Rothard, H.; da Silveira, E. F. Radiolysis of Astrophysical Ices by Heavy Ion Irradiation: Destruction Cross Section Measurement. *Low Temp. Phys.* 2012, *38*, 759.
(46) Mejia, C. F.; de Barros, A. L. F.; Bordalo, V.; da Silveira, E. F.; Boduch, P.; Domaracka, A.; Rothard, H. Cosmic Ray-Ice Interaction Studied by Radiolysis of 15 K Methane Ice with MeV O, Fe and Zn Ions. *Mon. Not. R. Astron. Soc.* 2013, *433*, 2368 − 2379.
(47) da Costa, C. A. P.; Souza-Corrêa, J. A.; da Silveira, E. F. Infrared Analysis of Glycine Dissociation by MeV Ions and KeV Electrons. *Mon. Not. R. Astron. Soc.* 2021, *502*, 2105 − 2119.
(48) Rothard, H.; Domaracka, A.; Boduch, P.; Palumbo, M. E.; Strazzulla, G.; da Silveira, E. F.; Dartois, E. Modification of Ices by Cosmic Rays and Solar Wind. *J. Phys. B: At., Mol. Opt. Phys.* 2017, *50*, No. 062001.
(49) Günzler, H.; Gremlich, H.-U. *IR Spectroscopy: An Introduction*; Wiley-VCH: Weinheim, 2002.
(50) Gerakines, P. A.; Schutte, W. A.; Ehrenfreund, P. Ultraviolet Processing of Interstellar Ice Analogs. *Astron. Astrophys.* 1996, *312*, 289 − 305.
(51) Seperuelo Duarte, E.; Domaracka, A.; Boduch, P.; Rothard, H.; Dartois, E.; da Silveira, E. F. Laboratory Simulation of Heavy-Ion Cosmic-Ray Interaction with Condensed CO. *Astron. Astrophys.* 2010, *512*, A71.
(52) Danger, G.; Bossa, J.-B.; de Marcellus, P.; Borget, F.; Duvernay, F.; Theule, P.; Chiavassa, T.; d'Hendecourt, L. Experimental Investigation of Nitrile Formation from VUV Photochemistry of Interstellar Ices Analogs: Acetonitrile and Amino Acetonitrile. *Astron. Astrophys.* 2011, *525*, A30.
(53) Lowenthal, M. S.; Khanna, R. K.; Moore, M. H. Infrared Spectrum of Solid Isocyanic Acid (HNCO): Vibrational Assignments and Integrated Band Intensities. *Spectrochim. Acta, Part A: Mol. Biomol. Spectrosc.* 2002, *58*, 73 − 78.
(54) Bethe, H. Zur Theorie des Durchgangs schneller Korpuskularstrahlen durch Materie. *Ann. Phys.* 1930, *397*, 325 − 400.
(55) Ziegler, J. F. Stopping of Energetic Light Ions in Elemental Matter. *J. Appl. Phys.* 1999, *85*, 1249 − 1272.
(56) Shen, C. J.; Greenberg, J. M.; Schutte, W. A.; van Dishoeck, E. F. Cosmic Ray Induced Explosive Chemical Desorption in Dense Clouds. *Astron. Astrophys.* 2004, *415*, 203 − 215.
(57) Webber, W. R.; Yushak, S. M. A Measurement of the Energy Spectra and Relative Abundance of the Cosmic-Ray H and He Isotopes over a Broad Energy Range. *Astrophys. J.* 1983, *275*, 391.
(58) Portugal, W.; Pilling, S.; Boduch, P.; Rothard, H.; Andrade, D. P. P. Radiolysis of Amino Acids by Heavy and Energetic Cosmic Ray Analogues in Simulated Space Environments: *a*-Glycine Zwitterion Form. *Mon. Not. R. Astron. Soc.* 2014, *441*, 3209 − 3225.